Protein adsorption on tailored substrates: long-range forces and conformational changes

2008 J. Phys.: Condens. Matter 20 404226

(http://iopscience.iop.org/0953-8984/20/40/404226)

J. Phys.: Condens. Matter **20** (2008) 404226 (11pp) doi:10.1088/0953-8984/20/40/404226

Protein adsorption on tailored substrates: long-range forces and conformational changes

M Bellion[1], L Santen[1], H Mantz[2], H Hähl[2], A Quinn[2], A Nagel[2], C Gilow[2], C Weitenberg[2], Y Schmitt[2] and K Jacobs[2]

[1] Department of Theoretical Physics, Saarland University, 66041 Saarbrücken, Germany
[2] Department of Experimental Physics, Saarland University, 66041 Saarbrücken, Germany

E-mail: k.jacobs@physik.uni-saarland.de

Received 15 May 2008, in final form 4 July 2008
Published 10 September 2008
Online at stacks.iop.org/JPhysCM/20/404226

Abstract
Adsorption of proteins onto solid surfaces is an everyday phenomenon that is not yet fully understood. To further the current understanding, we have performed *in situ* ellipsometry studies to reveal the adsorption kinetics of three different proteins, lysozyme, α-amylase and bovine serum albumin. As substrates we offer Si wafers with a controlled Si oxide layer thickness and a hydrophilic or hydrophobic surface functionalization, allowing the tailoring of the influence of short- and long-range interactions. Our studies show that not only the surface chemistry determines the properties of an adsorbed protein layer but also the van der Waals contributions of a composite substrate. We compare the experimental findings to results of a colloidal Monte Carlo approach that includes conformational changes of the adsorbed proteins induced by density fluctuations.

1. Introduction

The adsorption of proteins on the solid/liquid interface is not only a fundamental phenomenon, but it is also of great technical importance e.g. in biomedical engineering, as protein adsorption is the first step in integrating an implanted device into living tissue. Whenever a protein-containing solution (such as saliva) is brought into contact with a solid surface (e.g. teeth), the macromolecules adsorb spontaneously to the solid. The process is called unspecific adsorption, since specific lock-and-key mechanisms are absent [1, 2]. Upon adsorption, the protein conformation might be changed, which can even lead to a denaturation of the protein and hence a loss of biological activity [3–7]. A detailed characterization of the nature of the conformational changes is tricky, since the adsorbed protein film thickness is in the nanometre range and therefore only a minute amount of material can be probed. It is for this reason that conformational changes are typically characterized indirectly, either by recording a lack of biological activity or by changes in film thickness. In this study, we use ellipsometry to characterize film thickness or rather the amount of adsorbed protein over time. The knowledge, however, of why and how proteins behave upon adsorption, opens new pathways for the design of best-performing functional membranes, implant materials, tooth fillings etc.

The thermodynamic process of adsorption is governed by an interplay of short- and long-range interactions, as described in the Derjaguin–Landau–Verwey–Overbeek (DLVO) theory [8, 9]. The main players in the long-range interactions are van der Waals and Coulomb contributions. Usually, Coulomb interactions in physiological surroundings are strongly screened by buffer mechanisms, yet the van der Waals interactions are always present as they cannot be screened. In this study we will address the question if at all—for the dynamic process of protein adsorption—van der Waals forces play a significant role or if short-range and Coulomb interactions are the main actors. For three well-characterized proteins, α-amylase, lysozyme and bovine serum albumin (BSA), we record the adsorption kinetics by ellipsometry and compare the results with colloidal Monte Carlo simulations.

2. Experimental details

2.1. Materials

The proteins used in this study, α-amylase (product no. 10092), lysozyme (product no. 62971) and bovine serum albumin

Table 1. Substrate characterization results.

d (SiO) (nm)	Hydro-	rms (nm)	θ_a^{water}	θ_r^{water}	$\theta_a^{glycerol}$	$\theta_a^{1-bromonaphthalene}$
2	philic	0.09(2)	5(2)°	Complete wetting	11(3)°	13(4)°
192	philic	0.13(3)	7(2)°	Complete wetting	17(3)°	15(3)°
2	phobic	0.12(2)	111(1)°	107(1)°	95(2)°	62(4)°
192	phobic	0.15(2)	112(1)°	108(2)°	92(2)°	63(3)°

Table 2. Surface energies γ and their Lifshitz–van der Waals γ^{LW} and Lewis acid–base γ^{AB} components of the substrates, as determined by contact angle measurements, the results of which are listed in table 1.

d (SiO_2) (nm)	Hydro-	γ (mJ m^{-2})	γ^{LW} (mJ m^{-2})	γ^{AB} (mJ m^{-2})
2	philic	64.2	43.5	20.7
192	philic	63.2	43.1	20.1
2	phobic	24.1	24.1	0.0
192	phobic	23.6	23.6	0.0

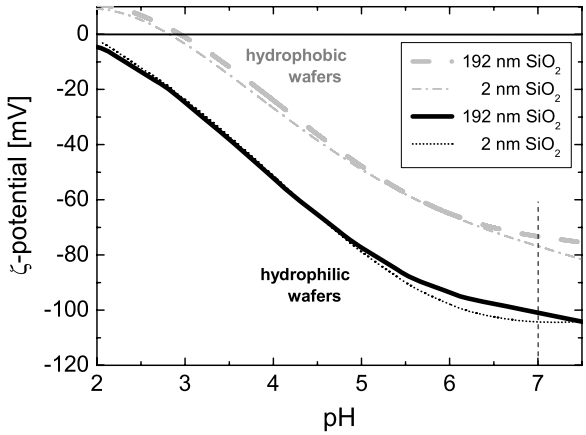

Figure 1. ζ-potential of hydrophobic and hydrophilic silicon wafers with thin and thick oxide layer as function of pH [25]. For the ζ-potential, differences in SiO_2 layer thickness are irrelevant. Note that adsorption experiments in this study have been performed at pH 7.0.

(product no. A3059) were purchased from Sigma-Aldrich, Steinheim, Germany. Lysozyme and α-amylase are proteins contained in the human saliva, where α-amylase is an enzyme able to split starch into maltose and is also known as a primary colonizer for bacteria in the human oral cavity leading to the formation of plaque [10, 11]. In the same environment, lysozyme exhibits an antibacterial effect [4]. The third protein of this study, BSA, was chosen for its known ability to switch conformation upon a change of the pH of a surrounding solution [12] and because of its similar size as compared to amylase, yet with a different isoelectric point. The isoelectric point of BSA is at pH 4.7 [13], that of amylase is at pH 6.5 [14] and for lysozyme it is reported to be at pH 11.0 [15].

As substrates, silicon wafers were used with natural (2 nm, Wacker Siltronic AG, Burghausen, Germany) and thermally grown (192 nm, Silchem, Freiberg, Germany) amorphous silicon dioxide surfaces (called thick and thin SiO_2 surfaces in the following). In their delivered state, residues from the polishing procedure (mostly hydrocarbons) prevent the surface from being completely wettable by water (0° contact angle). A 0° contact angle can only be reached by a thorough cleaning procedure. We therefore dip the Si wafers first for 30 min in fresh 1:1 H_2SO_4(conc.)/H_2O_2 (30%) solution. Subsequently, the acids were removed by rinsing the wafers for 60 min in hot deionized water, changing the water three to four times. All samples were prepared in a clean room (class 100) environment. Outside this environment, the receding water contact angle rapidly rises since e.g. dust particles act as pinning centres. All wafers termed 'hydrophilic' that were used for this study exhibit receding water contact angles of less than 10° before they were immersed into protein solutions, cf table 1 for details. By standard procedures [16, 17], using self-assembling silane molecules with a CH_3 tailgroup (octadecyl-trichlorosilane, OTS, purchased from Sigma-Aldrich, Germany), they can be hydrophobized yielding a second set of thick and thin SiO_2 substrates with altered surface properties. The obtained water contact angles of the hydrophobized wafers were larger than 110° with a hysteresis (i.e. the difference between advancing (θ_a) and receding (θ_r) contact angle) of less than 5° (cf table 1). In order to obtain the surface energies, additionally, glycerole and 1-bromonaphthalene were used for contact angle measurements. Together with the water contact angles, the Lifshitz–van der Waals and the Lewis acid–base components of the surface energy can be determined [18]. The results are listed in table 2.

The thickness of silicon oxide layers and the self-assembled monolayer (SAM) of OTS were measured via ellipsometry yielding the above mentioned values for the oxide layers and a thickness of 2.6(1) nm for the OTS-SAM, which reflects the length of the OTS molecule. The surface roughness of the four types of wafers was determined using atomic force microscopy (AFM). The measured RMS roughness in a scan area of 1 μm^2 for all types of wafers were below 0.2 nm.

Using these four types of substrates and keeping all other parameters (salt and protein concentration, pH and temperature) constant allows for a separation of effects due to the long-range and due to the short-range part of the surface potential [19–22]. A hydrophobization of the surfaces significantly alters the short-range forces and consequently the contact angle while the van der Waals forces are essentially kept constant [23]. A variation of the SiO_2 layer thickness, however, allows for a tuning of the long-range part of the potential only. In aqueous solution, the long-range part consists of a van der Waals and a Coulomb part. In order to reassure ourselves that Coulomb interactions are identical on wafers of thick and thin SiO_2 layers, ζ-potential measurements have been performed [24, 25]. The results are shown in figure 1. In the measured range of 2.0 $<$ pH $<$ 7.5, wafers with thick or

thin SiO_2 layers reveal, within the experimental error, identical values[3]. Comparing, however, the curves of hydrophilic and hydrophobic wafers, the hydrophilic wafers exhibit a stronger negatively charged surface.

These measurements corroborate the statement that a variation of the oxide layer thickness does not result in a change of the Coulomb part of the surface potential. The four different types of substrates are therefore ideally suited to reveal the influence of long-range van der Waals interactions on protein adsorption.

2.2. Adsorption studies by ellipsometry

Ellipsometry was used to determine the amount of adsorbed protein, either by *in situ* monitoring of the adsorption process or by *ex situ* measurements. Also the sample surfaces were inspected and ellipsometry revealed the OTS and the SiO_2 layer thickness. Ellipsometry and its use for the analysis of processes at biological interfaces are well described in literature, e.g. [26, 27]. To briefly summarize, this optical technique relies on the fact that the polarization state of light is altered upon reflection from a surface at oblique incidence. The two parameters measured via ellipsometry, Δ and Ψ are related to the complex reflection coefficients, R_s and R_p, for perpendicular and parallel polarized light respectively [28]:

$$\frac{R_p}{R_s} = \tan\Psi \exp(-\mathrm{i}\Delta). \tag{1}$$

The single wavelength ellipsometer (EP^3, Nanofilm, Göttingen, Germany) was operated in a PCSA (polarizer—compensator—sample—analyser) configuration at a wavelength of 532 nm. The ellipsometric angles Ψ and Δ were recorded via the nulling ellipsometry principle with a sampling rate of 1.5–6 min^{-1}. This rate allowed for an *in situ* measurement of the protein layers forming on the offered substrates.

In general it is not possible to calculate the physical properties of the reflecting surface from Δ and Ψ directly but from building an optical model [28]. Using single wavelength ellipsometry, one has to assume layers of constant thickness to get a reasonable result for the model parameters (refractive index and thickness of all layers). This is not the case for protein layers, as has been shown by many studies, involving e.g. atomic force microscopy (AFM) [29].

From the ellipsometric angles the thickness of the protein layer—assumed as homogeneous—was calculated via a model keeping the index of refraction of the layer constant. Since it is not possible to distinguish between a change in refractive index and in film thickness for layers below approximately 5 nm [28] we used de Feijter's method to determine the adsorbed mass Γ as a function of the refractive index n_f of the protein film and the film thickness d_f

$$\Gamma = d_\mathrm{f}\frac{n_\mathrm{f} - n_\mathrm{a}}{\mathrm{d}n/\mathrm{d}c}, \tag{2}$$

with n_a as the ambient refractive index. $\mathrm{d}n/\mathrm{d}c$ is the increment of the refractive index of the solution due to the increase of molecule concentration, where $n(c)$ was assumed to be a linear function with a fixed gradient of 0.183 cm^3 g^{-1} [30, 31].

For the measurements, the substrates were enclosed in a temperature controlled teflon fluid cell. This cell allowed ellipsometric measurements at angles of incidence of 65° and 70°. It was connected to a flow system which enabled constant flow rates to be maintained during the injection of a protein solution via a sample injector (Rheodyne Manual Sample Injector).

The proteins were dissolved in a 10 mM phosphate buffer solution (ionic strength $I = 20$ mM leading to a calculated Debye screening length of 2.2 nm) with a pH of 7.0. The same buffer was used to fill the microfluidic system prior to the injection of the protein. After reaching thermal equilibrium at 37 °C and a constant flow rate in the whole flow system, we obtained a constant baseline in the measured ellipsometric angles (which is not plotted here). Then, the adsorption measurements were started by the injection of the protein solution.

Additionally, stationary film thicknesses were recorded in a separate series of *ex situ* ellipsometry measurements. Here, the samples were exposed to buffer solutions with several different protein concentrations, while keeping all other parameters (temperature, pH, ionic strength, substrate preparation) constant. After 5 h, when the final protein layer thickness is expected to be reached (as deduced from the *in situ* ellipsometry measurements) the samples were taken out, rinsed in deionized water and dried in a very soft stream of pure nitrogen. That way, we expect only irreversibly adsorbed protein to stay on the surface. The film thickness was then measured by ellipsometry, using variable angles of incidence. For the evaluation of the data, the film was modelled as an effective medium owing to possible residual water incorporated in the film.

2.3. Results and discussion

The *in situ* ellipsometry experiments revealed a typical feature of the adsorption kinetics, cf figure 2: after a fast initial adsorption, a plateau value of the adsorbed amount is reached. In the case of lysozyme, the adsorption rate decreases continuously. This Langmuir-like adsorption behaviour was expected and is described in the literature [4]. The final layer thickness depends mostly on the surface chemistry of the offered surface. In the case of lysozyme, the effect of oxide layer thickness seems to be negligible. The higher amount of adsorbed protein on the hydrophilic samples can be understood in the following way: The adsorption took place at pH 7.0. There, lysozyme molecules with an isoelectric point at pH 11.0 [4] carry a positive net charge of $8e$ [32]. The hydrophilic SiO_2 surface, however, is with $-103(12)$ mV ζ-potential negatively charged at pH 7.0, cf figure 1. The hydrophobic surface at the same pH carries a ζ-potential of only $-75(12)$ mV. Since adsorption is promoted by attractive Coulomb interactions between surface and protein, a stronger adsorption is expected on the hydrophilic surface, which is indeed true for the lysozyme experiments.

In the case of α-amylase, the adsorption curves on the thick oxide wafers also show Langmuir-like adsorption

[3] For pH larger than 7.5, etching of the material starts to play a role. The effect is strongest on the hydrophilic 2 nm SiO_2 layer.

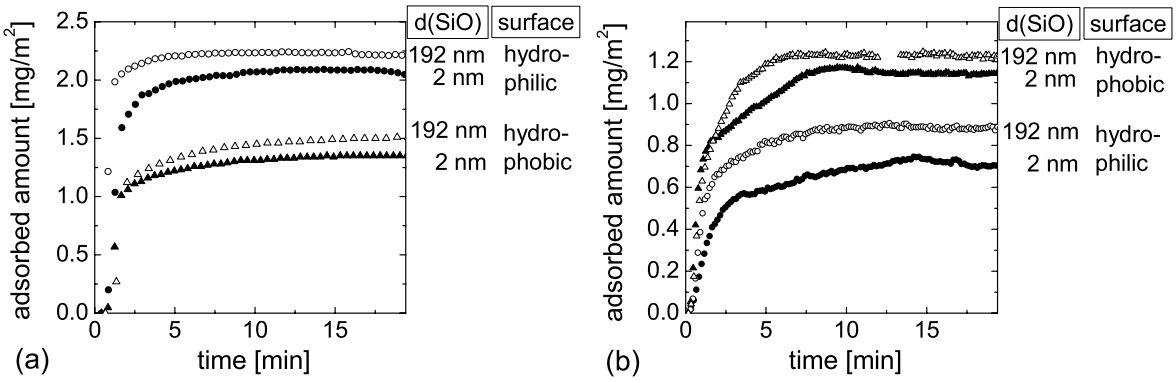

Figure 2. Adsorption kinetics of (a) lysozyme and (b) amylase on the four different types of surfaces.

characteristics [33]. Yet in the case of amylase on thin SiO_2 wafers, no matter whether hydrophilic or hydrophobic, two 'kinks' separate the initial fast adsorption from the constant signal at the late stage. Again, the final layer thickness depends only weakly on the SiO_2 thickness but on the hydrophilicity. Here, more protein is adsorbed on the hydrophobic surfaces. This can be explained via the hydrophobic effect. At pH 7, α-amylase (with its isoelectric point at pH 6.5 [14]) exhibits a net charge that is close to zero. Thus, Coulomb attraction plays a minor role and the hydrophobic interactions can dominate: the protein is attracted to the hydrophobic surface since that way the contact of water with the hydrophobic side groups of the proteins and the hydrophobic wafer surface is minimized. As mentioned above, a prominent feature of the adsorption kinetics of amylase on the thin SiO_2 wafers is a 'stepped' kinetics, regardless of their actual surface chemistry. Additional measurements revealed that this type of stepped kinetics can be recorded on Si wafers with SiO_2 thicknesses from 2 nm (lowest thickness studied) up to 20 nm [34].

A further test of the argument is to increase the ionic strength of the protein-containing buffer solution. Then, the attractive Coulomb interactions between the proteins and the surface should be screened more strongly and we therefore expect a lower adsorbed amount on the substrate's surface. This effect should be most prominent for lysozyme with its high isoelectric point. We therefore performed *ex situ* measurements on hydrophilic Si wafers with a thin SiO_2 layer, exposing them for 5 h to a lysozyme-containing buffer solution. A thorough rinse in deionized water ensures that only irreversibly bound proteins remain on the surface, as described before. The measurements were performed for several different protein concentrations and ionic strengths of the solution. As can be seen in figure 3, the absolute amount of irreversibly adsorbed lysozyme on the substrates decreases with increasing ionic strength (here from $I = 0.01$ M to $I = 0.2$ M referring to Debye screening lengths of 3.1–0.7 nm). We also observe an increase of the amount adsorbed with increasing protein concentration.

So far, we can explain the long-term adsorption behaviour of lysozyme and amylase, and all experimental results are consistent with the expectations, yet a reason for the kinks in the kinetics is still lacking. Why are stepped kinetics observed for amylase, but not for lysozyme?

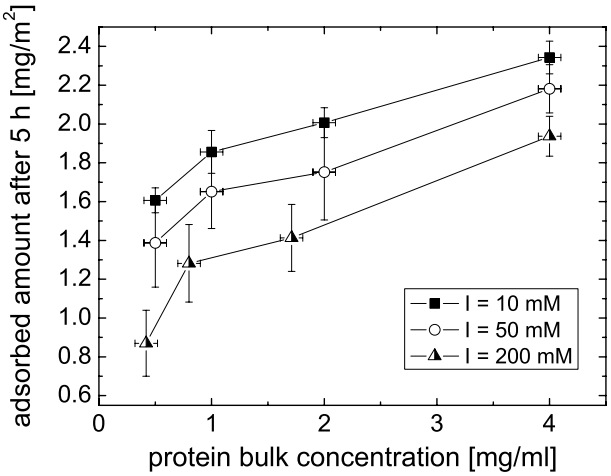

Figure 3. *Ex situ* measurements of the adsorbed amount of lysozyme onto hydrophilic Si wafers with 2 nm SiO_2 layer, after being exposed for 5 h to a protein-containing buffer solution. As a parameter, the ionic concentration I has been changed, resulting in a higher amount adsorbed at lower I, as expected.

The observation of such a stepped adsorption kinetics leads to the assumption that an additional process with a timescale relevant for these experiments must be involved. The hypothesis is thus that a change in the configuration of the tertiary structure of the molecule is responsible for the stepped kinetics.

As compared to such compact and small lysozyme molecules, α-amylase is known to be a 'soft' protein [4], possibly able to undergo a major configurational change upon adsorption. Such an ability is known from bovine serum albumin [12], a molecule of similar size as α-amylase. And indeed, also for BSA, stepped kinetics could be observed on the hydrophobized silicon wafers with thin SiO_2 (cf figure 4). The parameters for the surrounding solution (ionic strength, type of buffer, pH) were the same as for the experiments with α-amylase or lysozyme. A decrease of temperature from physiological 37.5 °C to room temperature results in a significantly prolonged 'linear' regime, i.e. the regime of constant adsorption rate. The initial adsorption is hereby only slowed down marginally. Interestingly, the kinks in the kinetics

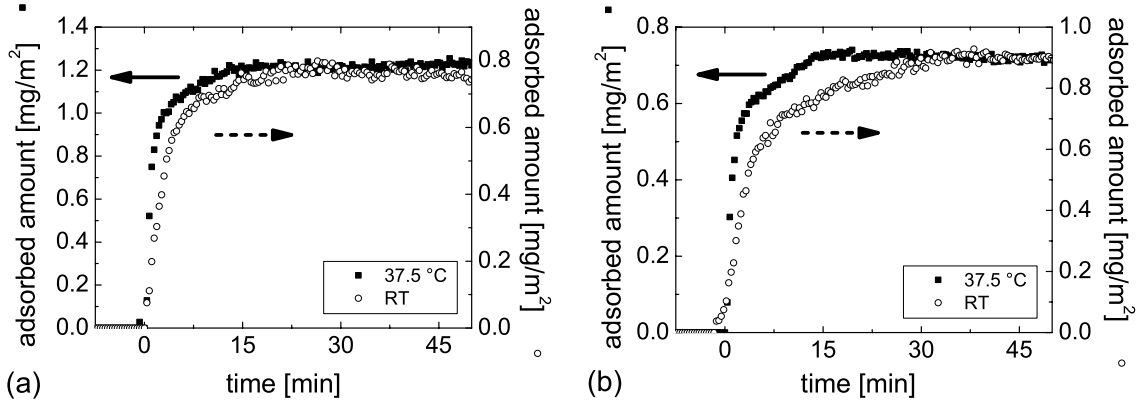

Figure 4. BSA adsorption kinetics on (a) thick and (b) thin SiO_2 layers at room temperature (RT) and 37.5 °C. Three-step kinetics can only be observed on wafers with thin layer thickness and the intermediate linear regime is more pronounced at T = RT.

still appear although the measurements were not performed near the proteins isoelectric point of pH 4.7 [15]. At the chosen pH of 7 also—here repulsive— Coulomb interactions are existent.

So far, the most striking experimental result is that the proteins are sensitive to van der Waals forces, as revealed by different adsorption kinetics. Effects for substrates of different surface charge state could be excluded by ζ-potential measurements. To further clarify the role of changes of the protein conformation during adsorption, we performed Monte Carlo simulations, as will be detailed in section 3.

3. Theoretical details

3.1. Modelling of the protein

Modelling of protein adsorption is a challenging task due to the large number of internal degrees of freedom, which determine the structure and orientation of the complex macromolecules. Additionally, the ambient solution, i.e. a large number of water molecules, and the surface structure have to be considered. Therefore a full atom simulation describing the adsorption of a protein film is not feasible on the relevant timescale, since so far simulations of single fully hydrolysed proteins are limited to a few nanoseconds, a time interval which is too short to predict structural changes upon adsorption [35].

A way to overcome these computational restrictions is given by coarse-grained models, allowing experimentally relevant timescales to be reached for many protein systems. Coarse-graining can be carried out on different length scales. Recently, models representing a few atoms by a single particle have been used [36], e.g. in the modelling of biological membranes [37]. Coarse-graining on this scale permits timescales to be reached that are relevant for structural changes for a small number of proteins. Modelling the adsorption of a complete protein layer, however, needs a further reduction of dynamical degrees of freedom. Our simulation model represents proteins as single particles, which may or may not carry an internal degree of freedom. Interactions between these model proteins are described in the framework of the DLVO-theory [8, 9], considering steric repulsion, van der Waals and Coulomb (electrical double layer) interactions. The van der Waals contribution of the interactions are calculated by using Hamaker's results [38], and the electrostatic forces acting on the model proteins can be approximated using the linear superposition approximation (LSA) [39] together with Sader's equation [40] for the effective far field potential. Using this approach the particle–surface interactions take the form (table 3 summarizes the abbreviations used in the following)

$$U_{\mathrm{ps}}(z) = U_{\mathrm{ps}}^{\mathrm{el}}(z) + U_{\mathrm{ps}}^{\mathrm{VdW}}(z) \tag{3}$$

where the van der Waals contribution (recognizing the substrate oxide layer of thickness H) is given by

$$U_{\mathrm{ps}}^{\mathrm{VdW}}(z) = -\frac{1}{6}\left\{\frac{A_{\mathrm{ps}}}{z-1} + \frac{A_{\mathrm{ps}}^{l}}{z-1+H}\right\} \tag{4}$$

and the electric double layer interaction by

$$U_{\mathrm{ps}}^{\mathrm{el}}(z) = B_{\mathrm{ps}}\,\mathrm{e}^{-\kappa a(z-1)} \tag{5}$$

where

$$B_{\mathrm{ps}} = a\left(\frac{4\pi\epsilon\epsilon_0 k_{\mathrm{B}}T}{e^2}\right)\left(\frac{\psi_p + 4\gamma\Omega\kappa a}{1+\Omega\kappa a}\right) \times \left(4\tanh\left(\frac{\psi_s}{4}\right)\right).$$

The bottom of the simulation volume is located at $z = 1.02$ (see figure 5, where the surface potential for the standard set of parameters takes the value $U_{\mathrm{ps}}(z = 1.02) = -27.56$). Similarly, the particle–particle interactions are given by

$$U_{\mathrm{pp}}(r) = U_{\mathrm{pp}}^{\mathrm{el}}(r) + U_{\mathrm{pp}}^{\mathrm{VdW}}(r) + U_{\mathrm{pp}}^{\mathrm{steric}}(r) \tag{6}$$

where the van der Waals contribution is given by

$$U_{\mathrm{pp}}^{\mathrm{VdW}}(r) = -\frac{A_{\mathrm{pp}}}{6}\left\{\frac{2}{r^2-4} + \frac{2}{r^2} + \ln\left(1-\frac{4}{r^2}\right)\right\} \tag{7}$$

and the electric double layer interaction by

$$U_{\mathrm{pp}}^{\mathrm{el}}(r) = \frac{B_{\mathrm{pp}}}{r}\,\mathrm{e}^{-\kappa a(r-2)} \tag{8}$$

Table 3. Standard values of the model parameters which are used if parameters are not explicitly given. Length scales are given in units of $a = 5$ nm, energies in units of k_BT.

Parameter	Symbol	Value
Radius in configuration A	a	5 nm
Temperature	T	310.65 K
System parameters		
Size of the simulation box	L_x	60
	L_y	60
	$L_{z,1}$	10
	$L_{z,2}$	10
Step-size	δ	0.1
Cutoff-radius	r_c	10
Chemical potential	μ	−91.5
De Broglie-wavelength	λ	4.43×10^{-13}
Interaction parameters		
Hamaker constants	A_{pp}	4.66
	A_{ps}	2.33
	A^l_{ps}	−3.50
Surface potential	ψ_p	0.414
	ψ_s	−3.734
Inverse Debye length	κa	1.59
Relative permittivity	ϵ	80.0
Parameters of steric interactions	F	10^{-7}
	g	6
Internal degree of freedom		
Relative particle size	Y	1.5
	Y^*	0.4
A priori probability	P	10^{-2}
Maximum distance	z^*	1.1
Surface potential	ψ_p^1	0.212

where

$$B_{pp} = a\left(\frac{4\pi\epsilon\epsilon_0 k_B T}{e^2}\right)\left(\frac{\psi_p + 4\gamma\Omega\kappa a}{1+\Omega\kappa a}\right)^2.$$

Finally the steric repulsions follow

$$U_{pp}^{steric}(r) = \frac{F}{(r-2)^g}. \quad (9)$$

The standard values of the model parameters are summarized in table 3.

Our approach neglects all structural details of the proteins including the distribution of charges and other details of the interactions which are relevant for very short distances between particles or particles and surface. The lack of accuracy at short distances is a general feature of the DLVO-theory, which is also true for colloidal systems, where the application of the DLVO-theory is well established. The strength of this approach is that the model parameters, e.g. protein net charge and Debye length, are experimentally accessible.

In order to study the adsorption kinetics, we applied a local Monte Carlo scheme. Although the Monte Carlo (MC) method does not explicitly describe the single-particle dynamics by integrating Newton's equations, we expect that the MC results are in good agreement with results from Brownian dynamics simulations. The advantage of MC is that internal degrees of freedom of the particles can easily be considered. This is of great importance for this application, since the denaturation of proteins upon adsorption has to be taken into account.

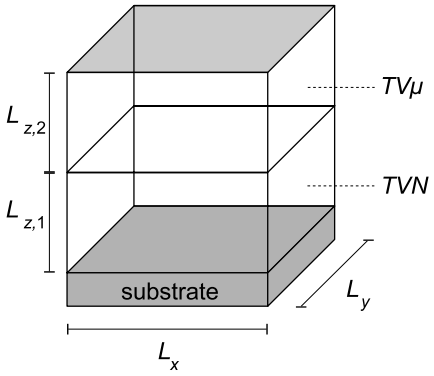

Figure 5. Structure of the simulation box.

The simulation is carried out in a volume (see figure 5) designed to represent the experimental setup. The experimental cavity is huge compared to the size of the proteins and also to the volume accessible in a computer simulation. Therefore deviations from the bulk behaviour are expected only in close proximity to the substrate. In the x- and y-direction, boundary effects can be neglected and periodic boundary conditions can be used.

We have divided the simulation volume into two parts (see figure 5) [41]. In the upper box a grandcanonical ensemble ($TV\mu$) is applied. The coupling to a particle reservoir allows us to keep a constant concentration of proteins throughout the simulation even in a small volume. In contrast, no particle exchange with an external reservoir is considered in the lower box, the one adjacent to the substrate. There, a conventional canonical ensemble (TVN) is applied. Particles can diffuse from the upper box into the lower one and vice versa. In the lower box, they are influenced by the attractive substrate. This results in a net particle flux from the upper into the lower box until a stationary state is reached. The total height of the simulation box is chosen such that a further increase of $L_{z,1}$ or $L_{z,2}$ does not change the simulation results qualitatively.

3.2. Modelling conformational changes

As there is experimental and theoretical evidence that proteins in the adsorbed state can undergo conformational changes [42, 43, 7], it is crucial for the adsorption kinetics whether the conformation of adsorbed proteins is stable.

In order to maintain the computational performance, we extended our model by introducing an internal degree of freedom, which models the different protein conformations. At the surface we distinguish between two states A and B: a marginally altered (native-like) conformation A or a substantially altered (denatured) conformation B. Conformational changes $A \rightarrow B$ are modelled to be reversible in order to account for the process of partial refolding upon denaturation [42, 43].

Trial probabilities are introduced for the thermally activated transitions $A \leftrightarrow B$. The denaturation upon

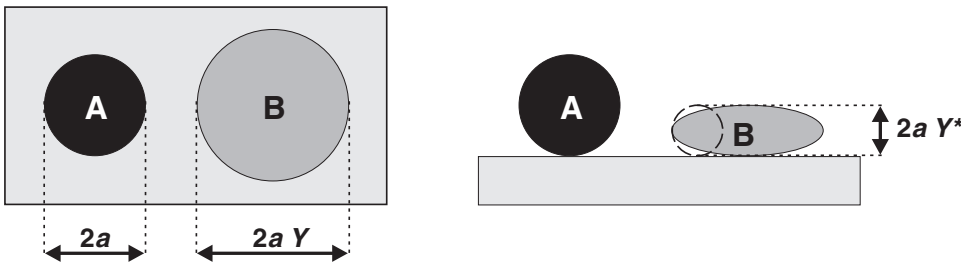

Figure 6. Effective particle size in different conformations. Left: diameter for particle–surface interactions in conformation B is $2aY$. Right: diameter for particle–particle interactions in conformation B is $2aY^*$.

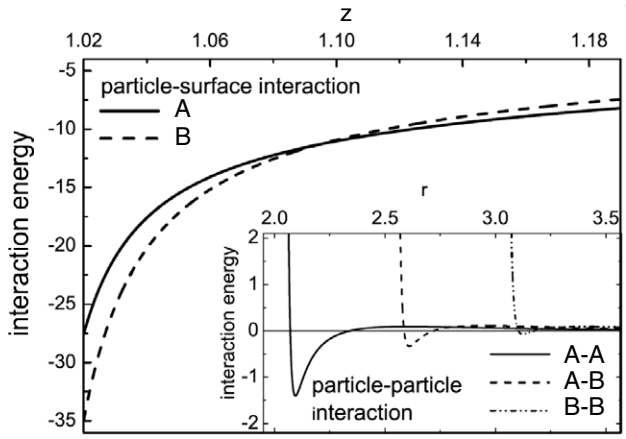

Figure 7. Conformation-dependent particle–surface and particle–particle (inset) potentials. z denotes the distance between the centre of a particle and the substrate surface; r is the centre-to-centre distance of two interacting particles. Energies are given in units of k_BT, z and r in units of the radius of the spheres in conformation A.

adsorption is associated with a larger contact area between the protein molecule and the substrate (spreading), thereby enlarging the binding energy of the proteins, cf figure 7. In the framework of the colloidal approach a conformational change of a protein molecule upon adsorption is represented by a volume conserving deformation of the particle. As a result the effective size of the particle ('particle interaction radius') with respect to its interaction with the substrate is increased, while it is reduced with respect to the particle–particle interactions. In order to maintain the computational efficiency, it is favourable to keep the spherical geometry of the particles. Consequently, the denaturation is implemented by adapting the particle interaction radii separately for the different contributions to the potentials (see the inset of figure 7). Note that particles in conformation B now cover a larger surface area of the substrate, cf figure 6. This way of modelling conformational changes is in the spirit of the equivalent sphere approach (ESA) for the interaction of non-spherical colloidal particles [44].

Introducing conformational changes, one has to modify the interactions as well. First, one has to consider the particle–surface interactions for conformation B. The structure of the potential

$$U_{\rm ps}^{B}(z) = U_{\rm ps}^{{\rm el},B}(z, B) + U_{\rm ps}^{{\rm VdW},B}(z) \tag{10}$$

is kept, but the van der Waals and electric double layer contributions are slightly modified. Now the van der Waals contribution is given by

$$U_{\rm ps}^{{\rm VdW},B}(z) = Y U_{\rm ps}^{\rm VdW}(z) \tag{11}$$

and the electric double layer interaction by

$$U_{\rm ps}^{\rm el}(z) = B_{\rm ps}^{B}\, {\rm e}^{-\kappa a(z-1)} \tag{12}$$

where

$$B_{\rm ps}^{B} = aY\left(\frac{4\pi\epsilon\epsilon_0 k_{\rm B}T}{e^2}\right)\left(\frac{\psi_p^1 + 4\gamma_1\Omega_1\kappa aY}{1+\Omega_1\kappa aY}\right)\left(4\tanh\left(\frac{\psi_s}{4}\right)\right)$$

and

$$\gamma_1 = \tanh(\psi_p^1/4), \qquad \Omega_1 = \frac{\psi_p^1 - 4\gamma_1}{2\gamma_1^3}.$$

Similarly, the particle–particle interactions for the different conformations are given by

$$U_{\rm pp}(r) = U_{\rm pp}^{\rm el}(r) + U_{\rm pp}^{\rm VdW}(r) + U_{\rm pp}^{\rm steric}(r). \tag{13}$$

The van der Waals $U_{\rm pp}^{\rm VdW}(r)$ contribution is given by

$$U_{\rm pp}^{\rm VdW}(r) = -\frac{A_{\rm pp}}{12}\left\{\frac{y}{x^2+xy+x} + \frac{y}{x^2+xy+x+y} + 2\ln\left(\frac{x^2+xy+x}{x^2+xy+x+y}\right)\right\} \tag{14}$$

where $x = (r-2)/2$ and $y = 1$ in the case of A–A interactions; $x = (r-Y-1)/2$, $y = Y^*$ in the case of A–B interactions, and $x = (r-2Y)/(2Y^*)$, $y = 1$ in the case of B–B interactions. The electric double layer interaction is given by

$$U_{\rm pp}^{{\rm el},ij}(r) = \frac{B_{\rm pp}^{ij}}{r}\,{\rm e}^{-\kappa a(r-a_i-a_j)} \tag{15}$$

where $B_{\rm pp}^{ij}$ is suitably adjusted (in analogy to the modification of $B_{\rm ps}$) and $a_i = 1$ ($a_i = Y$) if the particle is in conformation $A(B)$. Finally the steric repulsions between two particles is described by

$$U_{\rm pp}^{{\rm steric},ij}(r) = \frac{F}{(r-a_i-a_j)^g}. \tag{16}$$

Being surface-induced, the transition from compact to extended protein conformations takes place primarily only

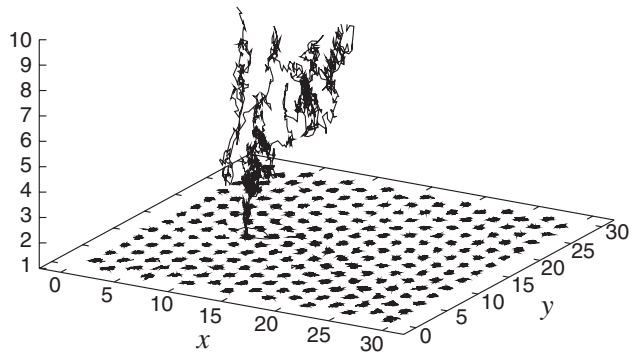

Figure 8. Typical trajectory of an adsorbing model protein at high surface coverage. Trajectories of adsorbed particles are also given during the same time interval. Other particles in solution are not shown.

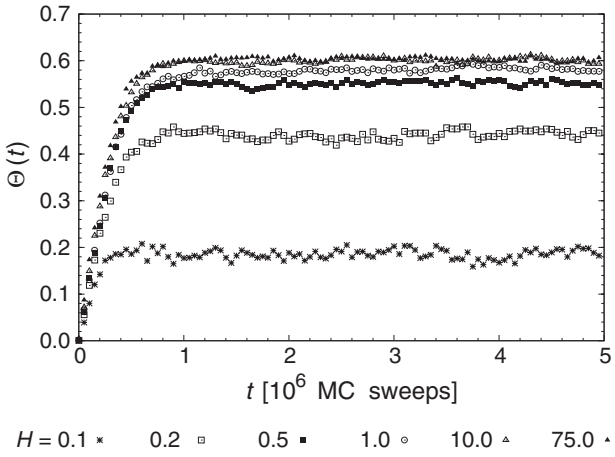

Figure 9. Surface coverage Θ as function of time (measured in MC sweeps) for different surface values of H. Parameters different from the standard set are $A^l_{\rm ps} = -5.0$ and $A_{\rm ps} = 1.0$.

close to the surface of the substrate. For simplicity, transitions $A \rightarrow B$ are restricted to particles that are in close proximity to the substrate, i.e. for $z \leqslant z^*$, where conformation B is energetically favoured (see figure 7). In contrast, conformational changes $B \rightarrow A$ are allowed in the entire simulation volume. This ensures that unbound particles are in the native conformation A.

3.3. Simulation results

In the framework of the *DLVO*-theory, the surface potential depends only on the z-coordinate, but this is only true for an empty surface. In the course of the adsorption process, translational invariance in the x- and y-direction is broken due to the presence of adsorbed proteins. For larger surface coverages this results in a non-trivial structure of surface potential in the x- and y-direction.

Figure 8 shows that this way of structuring the surface potential leads to a strong lateral confinement of the particles before adsorbing onto the substrate. This early alignment of the proteins is of great importance for the adsorption kinetics of the proteins, since it strongly enhances the efficiency of adsorption, compared to a random choice of positions, which is used in random-sequential-adsorption methods. For non-spherical particles, these results also indicate that previously adsorbed particles not only determine the position of the adsorbing proteins, but also their orientation close to the surface.

Using this modelling approach we can measure the adsorption kinetics of the model proteins. Consistent with the experimental findings, we observe the adsorption of a protein monolayer. By varying the Hamaker constants, it is possible to switch between reversible and irreversible adsorption. Figure 9 shows the time dependence of the surface coverages $\theta(t) = \frac{\pi}{L_x L_y} N_{\rm ad}(t)$ for the choices $A^l_{\rm ps} = -5.0$ and $A_{\rm ps} = 1.0$ which is proportional to the number of adsorbed particles per surface area (for definition of $L_{x,y}$, cf figure 5) and corresponds to the experimentally observed adsorbed amount Γ. Both choices of $A_{\rm ps}$ lead to reversible protein adsorption, whereby the crossover from the transient regime to the equilibrium coverage is rather sharp. Qualitatively, the time evolution of the surface coverage can be divided into a regime of fast initial adsorption, characterized by a linear increase of the adsorbed amount, and a stationary regime, where the coverage is fluctuating around the equilibrium value. This form of the adsorption kinetics has also been obtained in the case of irreversible adsorption, which we observe for $A_{\rm ps} = 4.66$ and $A^l_{\rm ps} = -3.50$.

Differences between reversible and irreversible processes originate in the formation of an ordered structure slowing down the saturation of surface coverage. Compared to reversible adsorption the maximal coverage is much higher and leads ultimately to the formation of a perfect two-dimensional crystal.

We notice that we obtain a 'conventional' shape of the adsorption kinetics characterized by a gradual reduction of the adsorption rate (see dashed curve in figure 10) for both choices of the Hamaker constants. The robustness of this result indicates that the model has to be extended in order to reproduce the observed three-step kinetics. In the experiments the long-range forces originating from the substrate turn out to change the adsorption kinetics qualitatively. Considering the trajectories of the model proteins, we expect that the long-range interactions influence the orientation of adsorbing protein molecules in solution, and consequently their initial conformation in the irreversible adsorption process. This physical picture implies that, depending on the nature of the long-range forces, different initial conformations of the adsorbed proteins are possible.

Figure 10 shows the time evolution of the surface coverage for irreversible adsorption kinetics. Compared to the reference curve (without conformational changes), the adsorption kinetics is characterized by an intermediate region with a moderate adsorption rate. In qualitative agreement with the experimental results, three regimes of the adsorption kinetics can be distinguished: During the first part of the kinetics the number $N_{{\rm ad},B}$ of adsorbed particles in conformation B grows almost as fast as the total number $N_{\rm ad}$ of adsorbed particles (see inset of figure 10), because at low surface coverages the particles transform immediately after

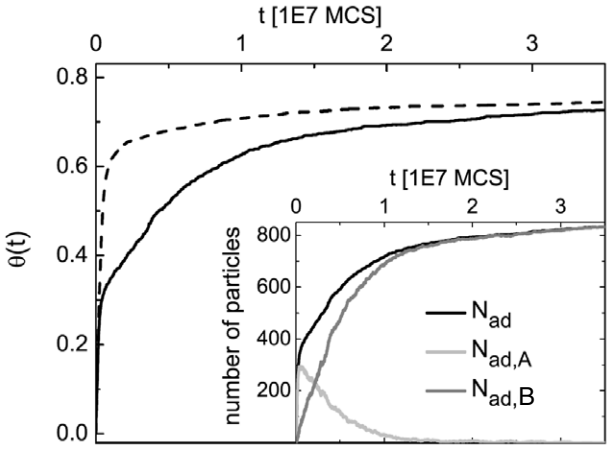

Figure 10. Irreversible adsorption kinetics for particles with (solid line) and without (dashed line) internal degree of freedom. Time t is measured in MC sweeps. Inset: Number of adsorbed particles depending on conformation.

adsorption to the energetically favoured conformation B (see figures 11(a) and (b)). With increasing surface coverage, i.e. for coverages similar to random closed packing for disks, the particle–particle interactions become more relevant and induce the growth of A-domains at the surface (see figures 11(c) and (d)). For these high surface coverages the optimization of particle–particle interactions due to the formation of A-domains overcompensates the unfavourable surface–particle interaction of conformation A. The third step of the adsorption kinetics can be viewed as the ordering transition of a 2d monodisperse system (see figures 11(e) and (f)), analogous to the system without internal degree of freedom.

Thus, according to the model presented, the occurrence of the discontinuity and the second linear regime in the adsorption kinetics can be ascribed to a collective transition in the internal degree of freedom of the particles, namely from a conformation that is stable on the single-particle level (B) to a conformation that optimizes the adsorbed amount at the surface (A). Discrepancies between the simulated adsorption kinetics and the experimental data for large times are inherent in the colloidal model.

The collective transition is observed for a wide range of realistic model parameters. Whether or not the effect of surface-induced conformational changes leads to a second linear regime in the adsorption kinetics, depends on how fast the collective transition takes place. The swiftness of the transition is given by the decrease of $N_{\mathrm{ad},B}$ and is influenced by several simulation parameters, e.g. the particle density, the timescale of the internal degree of freedom, the ratio of the effective particle radii and the relative strength of the conformation-dependent particle–particle and particle–surface interactions. The model results suggest the following consequences for real proteins: we expect the three-step kinetics to take place if the proteins are (i) able to diffuse at the surface and (ii) able to perform significant conformational changes at the surface, which implies a certain flexibility of the proteins.

In order to obtain a more comprehensive characterization of the biofilm, structural information should be provided as well. This is, at least in principle, possible by using atomic force microscopy (AFM), which allows one to obtain a high resolution surface profile. While the AFM measurements of solid surfaces are now well established, the characterization of (bio)polymer films is more difficult, since even in non-contact mode it is possible that the tip interacts with the biofilm and molecules are removed from the surface. Therefore linker molecules are often used in order to stabilize the biofilm against such interactions. These molecules are able to bind side chains of the protein, such that proteins go below the entropically favoured distance. This effect can be modelled by adding an attractive short-ranged potential to the particle–particle interactions and a reduction of the effective particle

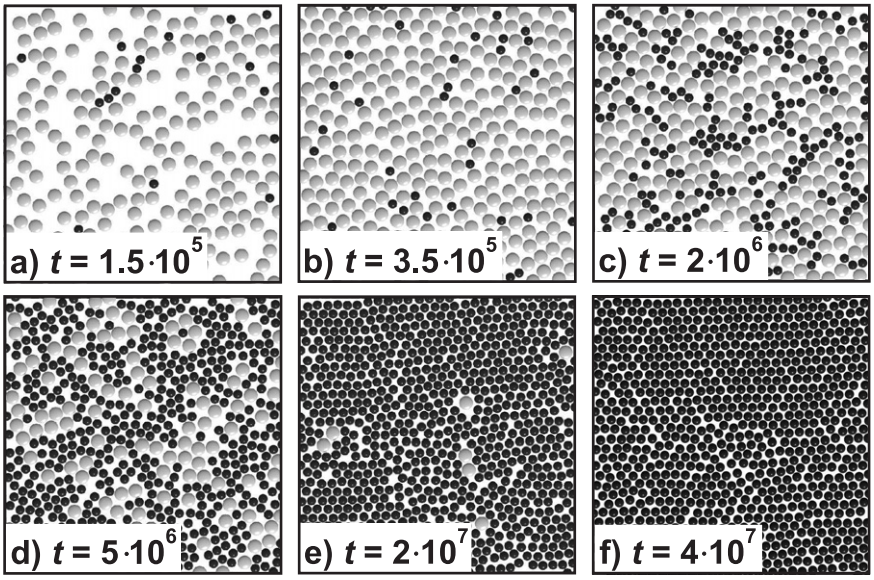

Figure 11. Snapshots of the adsorption layer. The dark (bright) particles represent model proteins in conformation $A(B)$.

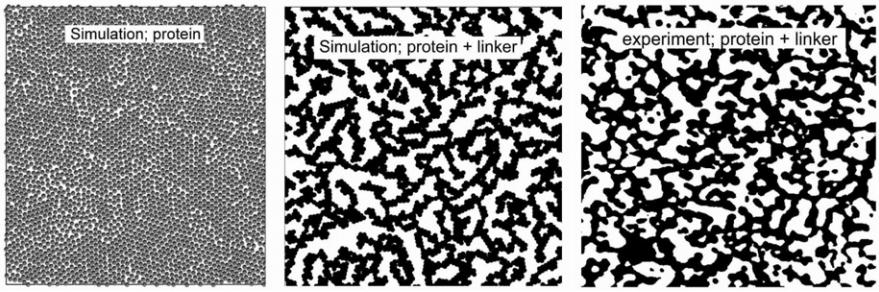

Figure 12. Studying the effect of adding linker molecules for a stabilization of a protein film (a frequent method to achieve robust biofilms for subsequent analysis). Left: initial configuration obtained from a simulation using the standard form of the interactions. Middle: stationary configuration in the computer simulation after adding a short-ranged contribution to the particle–particle interactions (which mimics the effect of a linker protein). Right: experimental view of an amylase film stabilized by glutaraldehyde. For a simple comparison with the simulations, a threshold has been applied to the height scale such that protein is black and substrate is white. Scan size is 500 nm.

size. Figure 12 shows that experimental and simulation results agree quite well. Regarding, however, the initial configuration before using the linker protein, it is obvious that fixation strongly alters the structure of the protein film. These results indicate that the *in situ* characterization of biofilms consisting of proteins that are mobile at the surface is still challenging.

4. Discussion and conclusion

In the present work, the role of long-ranged interactions for the adsorption of biofilms is discussed. We have been able to show that the properties of protein films are strongly influenced by the long-range van der Waals forces. Next to the adsorbed amount at the stationary state, the long-range part of the surface potential may even qualitatively change the adsorption kinetics. For amylase and for BSA, both rather large and flexible proteins and known to be able to undergo conformational changes, one observes a three-step kinetics. In order to elucidate the underlying mechanism, a theoretical approach has been used, describing proteins as colloidal particles, which can undergo changes of their effective size.

The introduction of the internal degree of freedom led to three dynamical regimes as experimentally observed: at low densities, enough surface per particle is available such that the proteins take on a wide spread conformation. After the surface coverage has reached a value that is comparable to random close packing, density fluctuations are able to stimulate transitions to more compact protein conformations (CPC). At high densities the CPCs are stable, since the gain in particle–particle interactions overcompensates the loss of free energy of the particle–surface contribution. Further adsorption then leads to growing CPC domains until the wide spread conformations are almost disposed. This process is followed by the saturation of the surface coverage.

The formation of CPC domains is determined by the structural stability of the adsorbed proteins and their mobility at the surface. Quantitative results of diffusivity and the free energy landscape of the adsorbed proteins are difficult to obtain. Experimental data for the diffusivity for different protein-substrate combinations vary considerably, but suggest a non-vanishing value of the diffusion constant for the experimental setup used in this paper (e.g. [4]). In addition to this, the temperature dependence of the observed adsorption kinetics is consistent with the physical picture: at lower temperature the diffusivity of the proteins is reduced and the structural stability increased. This leads, as theoretically expected, to a reduced slope of the second linear regime of the adsorption kinetics.

Although the colloidal approach offers a physical picture which is in qualitative agreement with the experimental findings, a number of questions are still left open. The experimentally observed fast saturation of the surface coverage combined with irreversible adsorption indicates that the modelling approach is so far incomplete. Therefore, it would be ideal to use more detailed and specific information, e.g. about the polar groups of the modelled protein. A promising theoretical approach for a refinement of the colloidal model is offered by coarse-grained molecular dynamic simulations, which are able to reach timescales relevant for the structural relaxation of the proteins at the surface, including e.g. denaturation. The ultimate goal of this multi-scale modelling approach is a quantitative description of biofilms on surfaces.

Experimentally, one aims at characterizing the local structure of the biofilms and at recording conformational changes *in situ*. Methods like atomic force microscopy have successfully been applied to stabilized protein layers, and an extension to a controlled *in situ* monitoring is under way. For instance, one can probe the spatial statistics of the adsorbed proteins at the surface. The influence of the scanning tip, however, might limit the applicability of the method to systems that are robust against density fluctuations. In the other systems, tip/protein interaction may alter the morphology of the biofilm. Moreover, powerful x-ray sources should in the near future be able to resolve conformational changes upon adsorption *in situ*. Also surface plasmon resonance spectroscopy or total internal reflection ellipsometry can reveal conformational changes, but for technical reasons, the choice of substrates is limited to noble metal layers.

Acknowledgments

The authors acknowledge financial support from the German Science Foundation under grant numbers GRK 1276 and

GRK 532 and from the Alexander von Humboldt Foundation, as well as technical support by Wacker Siltronic AG, Burghausen, Germany.

References

[1] Norde W 1986 *Adv. Colloid Interface Sci.* **25** 267
[2] Haynes C A and Norde W 1994 *Colloid Surf.* B **2** 517
[3] Engel M F M, Visser A J W G and van Mierlo C P M 2004 *Proc. Natl Acad. Sci.* **101** 11316
[4] Malmsten M 2003 *Biopolymers at Interfaces* (New York: Dekker)
[5] Gray J J 2004 *Curr. Opin. Struct. Biol.* **14** 110
[6] Keselowsky B G, Collard D M and Garcia A J 2005 *Proc. Natl Acad. Sci.* **102** 5953
[7] Michael K E, Vernekar V N, Keselowsky B G, Meredith J C, Latour R A and Garcia A J 2003 *Langmuir* **19** 8033
[8] Verwey E J W and Overbeek J T G 2000 *Theory of the Stability of Lyophobic Colloids* (New York: Dover)
[9] Derjaguin B and Landau L 1941 *Acta Physicochim. URSS* **14** 633
[10] Rogers J D, Palmer J R, Kolenbrander P E and Scannapieco F A 2001 *Infect. Immun.* **69** 7046
[11] Hannig M and Joiner A 2006 The structure, function and properties of the acquired pellicle *The Teeth and Their Environment* (*Monogr. Oral Sci.* vol 19) ed R M Duckworth (Karger: Basel) pp 29–64
[12] Foster J 1977 *Albumin Structure, Function and Uses* (Oxford: Pergamon) pp 53–84
[13] Arnebrandt T 2003 *Biopolymers at Interfaces* (New York: Dekker) pp 811–55
[14] Hu S, Xie M Y, Ramachandran P, Loo R R O, Li Y, Loo J A and Wong D T 2005 *Proteomics* **5** 1714–28
[15] Malamud D and Drysdale J W 1978 *Anal. Biochem.* **86** 620
[16] Wasserman S R, Whitesides G M, Tidswell I M, Ocko B M, Pershan P S and Axe J D 1989 *J. Am. Chem. Soc.* **111** 5852
[17] Brzoska J B, Azouz I B and Rondelez F 1994 *Langmuir* **10** 4367
[18] Mykhaylyk T A, Evans S D, Fernyhough C M, Hamley I W and Henderson J R 2003 *J. Colloid Interface Sci.* **260** 234
[19] Seemann R, Herminghaus S and Jacobs K 2001 *Phys. Rev. Lett.* **86** 5534
[20] Seemann R, Herminghaus S and Jacobs K 2001 *J. Phys.: Condens. Matter* **13** 4925
[21] Seemann R, Herminghaus S, Neto C, Schlagowski S, Podzimek D, Konrad R, Mantz H and Jacobs K 2005 *J. Phys.: Condens. Matter* **17** S267
[22] Huber G, Mantz H, Spolenak R, Mecke K, Jacobs K, Gorb N S and Arzt E 2005 *Proc. Natl Acad. Sci.* **102** 16293
[23] Israelachvili J 1991 *Intermolecular and Surface Forces* (London: Academic)
[24] Zimmermann R, Dukhin S and Werner C 2001 *J. Phys. Chem.* B **105** 8544
[25] Zimmermann R, private communication, in preparation
[26] Cuypers P A 1983 *J. Biol. Chem.* **258** 2426
[27] Vörös J 2004 *Biophys. J.* **87** 553
[28] Azzam R M A and Bashara N M 1977 *Ellipsometry and Polarized Light* (Amsterdam: North-Holland)
[29] Mulheran P A, Pellenc R, Bennett R, Green R J and Sperring M 2008 *Phys. Rev. Lett.* **100** 068102
[30] de Feijter J A, Benjamins J and Veer F A 1978 *Biopolymers* **17** 1759
[31] Ball V and Ramsden J J 1998 *Biopolymers* **46** 489
[32] Roth C M and Lenhoff A M 1995 *Langmuir* **11** 3500–9
[33] Quinn A, Mantz H, Jacobs K, Bellion M and Santen L 2008 *Europhys. Lett.* **81** 56003
[34] Mantz H *et al* 2008 at press
[35] Raffaini G and Ganazzoli F 2004 *Langmuir* **20** 3371
[36] Tozzini V 2005 *Curr. Opin. Struct. Biol.* **15** 144
[37] Reinwar B J, Illya G, Harmandaris V A, Müller M M, Kremer K and Deserno M 2007 *Nature* **447** 461
[38] Hamaker H C 1937 *Physics* **4** 1058
[39] Bell G M, Levine S and McCartney L N 1970 *J. Colloid Interface Sci.* **33** 335
[40] Sader J E 1997 *J. Colloid Interface Sci.* **188** 508
[41] Oberholzer M R, Wagner N J and Lenhoff A M 1997 *J. Chem. Phys.* **107** 9157
[42] Zhdanov V P and Kasemo B 2001 *Proteins* **42** 481
[43] Castells V, Yang S and Van Tassel P R 2002 *Phys. Rev.* E **65** 031912
[44] Adamczyk Z and Weronski P 1995 *Langmuir* **11** 4400